Published in "Journal of Raman Spectroscopy, 2010
doi: 10.1002/jrs.2572" which should be cited to refer to this work.

The aqueous Raman optical activity spectra of 4(*R*)-hydroxyproline: theory and experiment

Magdalena Pecul,[a,b]* Christine Deillon,[c] Andreas J. Thorvaldsen[b] and Kenneth Ruud[b]

Vibrational Raman optical activity (ROA) spectra have been measured for aqueous solutions of 4(*R*)-hydroxyproline at three different pH values and are compared with theoretical results calculated for several conformations of anionic, cationic and zwitterionic 4(*R*)-hydroxyproline using density functional theory (DFT) and the polarizable continuum model (PCM). The experimental ROA bands have been ascribed to the normal modes by comparison of the experimental and calculated vibrational frequencies and ROA intensities. Overall, using PCM for geometry optimization and force field calculations gives simulated Raman and ROA spectra that agree with the main features of the experimental spectra, whereas using PCM also in the calculations of optical tensors seems more problematic.

Keywords: Raman optical activity; amino acids; *ab initio* calculations; polarizable continuum model; pH effects

Introduction

Vibrational Raman optical activity (ROA) spectroscopy is based on the phenomenon of inelastic scattering of circularly polarized light by chiral molecules. It is measured as the difference in intensity of the right and left circularly polarized scattered Raman light. This effect was predicted and its existence demonstrated by Barron *et al*.[1,2] in the early 1970s. Until recently, the technique was to some extent a scientific curiosity. However, it has been gaining importance in the last few years, especially in the field of biochemistry, partly because of developments in the experimental technique, such as the cancellation of offsets by subtracting the spectra measured for the actual chiral molecule and that of its virtual, optically generated antipode.[3] ROA spectra are very sensitive to molecular conformation and – since the majority of biologically active molecules, and in particular biopolymers, are chiral – ROA spectroscopy is potentially a powerful tool in biophysics, biochemistry and structural biology.

One of the most important applications of ROA is the investigation of protein folding and of structure and dynamics of nucleic acids. Application of ROA in molecular biophysics enables us to characterize transition states of proteins with respect to both basic motifs of their secondary structure and spatial packing.[4–11] ROA spectra are being used to characterize secondary and tertiary structures of proteins[4,11] and there have been attempts to utilize the technique also for nucleic acids.[12,13] However, the relation between the ROA spectrum and the molecular conformation is complex, and it is difficult to derive simple empirical correlations between them. In such cases, *ab initio* studies can be very helpful.

Another field which calls for cooperation between experimental ROA spectroscopists and computational chemists is the assignment of absolute configurations by means of ROA.[14–16] ROA spectra coupled with theoretical calculations also allow us to obtain additional information on the vibrational spectra, since bands which coalesce in conventional Raman spectra may have different signs in their right and left circular polarization intensities, and therefore be separable in a ROA spectrum.

The first complete *ab initio* simulation of an ROA spectrum was presented by Polavarapu[17] in 1990 using the static approximation of Amos.[18] The first correlated calculations using multiconfigurational self-consistent field (MCSCF) wave functions and London atomic orbitals were presented 4 years later,[19] where also frequency-dependent optical tensors were employed. Nowadays, other computational techniques are available, including time-dependent density functional theory (DFT).[20,21] Much progress has recently been made in making *ab initio* calculations of ROA spectra a standard computational tool,[20–27] as reviewed elsewhere.[28–30]

The most important factor preventing large-scale *ab initio* calculations of ROA spectra has been the need for numerical differentiation of optical tensors with respect to nuclear displacements in order to evaluate ROA intensities in the double-harmonic approximation. However, two complementary approaches that allow for analytic calculations of the geometrical derivative of the relevant polarizabilities have recently been presented, first by Champagne and coworkers,[31–33] and very recently also by Thorvaldsen *et al*.[34,35]

ROA intensities, like all chiroptical properties,[36] appear to depend significantly on the molecular environment,[24] in particular

* *Correspondence to: Magdalena Pecul, Faculty of Chemistry, University of Warsaw, Pasteura 1, 02-093 Warszawa, Poland. E-mail: mpecul@chem.uw.edu.pl*

a *Faculty of Chemistry, University of Warsaw, Pasteura 1, 02-093 Warszawa, Poland*

b *Centre for Theoretical and Computational Chemistry, Department of Chemistry, University of Tromsø, N-9037 Tromsø, Norway*

c *Department of Physical Chemistry, University of Fribourg, Pérolles, CH-1700 Fribourg, Switzerland*

on the solvent. This poses a challenge for theoretical simulations. One technique used to deal with the problem of solvent effects is the polarizable continuum model (PCM), in which a solvent is treated as a uniform, polarizable dielectric continuum. In the present paper, we test the applicability of PCM to simulate aqueous environments. Another point we address by means of the combination of experimental and theoretical methods, is the influence of pH on the ROA spectra of amino acids.

Amino acids, the building blocks of proteins, are a frequent subject of experimental ROA spectroscopy. The experimental ROA spectra of proline has been recorded in H_2O and D_2O solutions by Kapitán *et al.*,[37] and a complete vibrational assignment was suggested on the basis of theoretical calculations. In this article, we present for the first time a combined experimental and theoretical study of the ROA spectra of 4(*R*)-hydroxyproline. Experimental ROA spectra have been collected for aqueous solutions at three different pH values. *Ab initio* results have been obtained for a number of conformers of the anionic, cationic and zwitterionic 4(*R*)-hydroxyproline. The main purpose of this work is to test the applicability of DFT/Hartree–Fock calculations combined with the PCM model for the solvent in predicting the ROA spectrum of a flexible, fairly complicated and hydrogen-bond-forming molecule.

The remaining part of the paper is organized as follows. First, the theory underlying the calculation of ROA is briefly outlined together with the computational details, followed by the experimental details. The results of the calculations and measurements are reported in the next section: the optimized structures of the molecules under study are described, and the experimental and calculated ROA spectra are discussed. Finally, the results are summarized and some concluding remarks are given.

Methodology

Theory and computational details

The measured ROA signal is the difference in intensity of the backward ($\pi = 180^\circ$) scattered signal between right ($I_R(\pi)$) and left ($I_L(\pi)$) circularly polarized light. The difference can be calculated as[1,38]

$$I_R(\pi) - I_L(\pi) = 24\beta(G')^2 + 8\beta(A)^2, \tag{1}$$

where

$$\beta(G')^2 = \sum_{ik} \frac{3\alpha^v_{ki}G'^v_{ki} - \alpha^v_{kk}G'^v_{ii}}{2} \tag{2}$$

$$\beta(A)^2 = \sum_{ijkl} \frac{1}{2}\omega_{\mathrm{rad}}\alpha^v_{ki}\epsilon_{kjl}A^v_{jli} \tag{3}$$

ω_{rad} is here the radiation's angular frequency and ϵ_{kjl} is the unit third-rank antisymmetric Levi–Civita tensor. In the presented data, $I_R(\pi) - I_L(\pi)$ has been multiplied by the Boltzmann factor $\exp(-\hbar\omega/kT)$ (where ω is the frequency associated with the vibrational transition and $\hbar$ and k are the Planck and Boltzmann constants, respectively) calculated for the temperature $T = 298$ K. Within the double harmonic approximation, G'^v_{ij} and A^v_{ijk} are derivatives of the imaginary part of the electric dipole–magnetic dipole polarizability $\mathbf{G}'$, and the real part of the electric-dipole–electric quadrupole polarizability $\mathbf{A}$[38] with respect to the normal coordinate of the vibration under study.

In the case of the gas-phase calculations, we have used the recently developed atomic orbital-based scheme for analytic calculations of the ROA circular intensity differences.[35,29] The approach is based on a general framework for the calculation of higher-order molecular properties for basis sets which may be both time and perturbation dependent.[34] The approach uses as a starting point the quasi-energy derivative with respect to a nuclear displacement (the quasi-energy gradient), which can be expressed in terms of the density matrix in the atomic-orbital basis as

$$Q^g = \frac{dQ}{dg} = \left\{ \frac{\partial \tilde{E}(\mathbf{D})}{\partial g} - \mathrm{Tr}\mathbf{S}^g\mathbf{W} \right\}_t, \tag{4}$$

where we have introduced the short-hand notation $A^b = \frac{dA}{db}$ for derivatives, and $\{\ldots\}_t$ indicates that we have performed a time averaging over a full period of the applied electromagnetic field (or equivalently: over all time). In the equation, we have also introduced the density matrix $\mathbf{D}$ in the atomic orbital basis, the generalized (time-dependent) self-consistent field (SCF) energy of the system, $\tilde{E}(\mathbf{D})$, its transposed partial derivative, the generalized (time-dependent) Fock matrix in the AO basis $\tilde{\mathbf{F}}$, and the energy–frequency-weighted density matrix $\mathbf{W}$, all quantities defined as

$$\tilde{E}(\mathbf{D}) = h_{\mathrm{nuc}} + v_{\mathrm{nuc}} + \mathrm{Tr}\left(\mathbf{h} - \frac{i}{2}\mathbf{T} + \mathbf{V}\right)\mathbf{D} + \mathrm{Tr}\,\frac{1}{2}\mathbf{G}(\mathbf{D})\mathbf{D}, \tag{5}$$

$$\tilde{\mathbf{F}} = \frac{\partial \tilde{E}(\mathbf{D})}{\partial \mathbf{D}^T} = \mathbf{h} + \mathbf{V} - \frac{i}{2}\mathbf{T} + \mathbf{G}(\mathbf{D}), \tag{6}$$

$$\mathbf{W} = \mathbf{D}\tilde{\mathbf{F}}\mathbf{D} + \frac{i}{2}\dot{\mathbf{D}}\mathbf{S}\mathbf{D} - \frac{i}{2}\mathbf{D}\mathbf{S}\dot{\mathbf{D}}, \qquad \dot{\mathbf{D}} = \frac{d}{dt}\mathbf{D}, \tag{7}$$

respectively. $\mathbf{S}$ is here the conventional overlap matrix, $\mathbf{S}^g$ the geometry-differentiated overlap matrix, and $\mathbf{T}$ an antisymmetric time-differentiated overlap matrix

$$S^g_{\mu\nu} = \frac{\partial S_{\mu\nu}}{\partial g} = \frac{\partial}{\partial g}\langle\chi_\mu|\chi_\nu\rangle,$$
$$T_{\mu\nu} = \langle\chi_\mu|\dot{\chi}_\nu\rangle - \langle\dot{\chi}_\mu|\chi_\nu\rangle, \qquad \dot{\chi}_\mu = \frac{d}{dt}\chi_\mu. \tag{9}$$

h_{nuc} is the nuclear repulsion energy, $\mathbf{h}$ is the integral matrix of the conventional one-electron operator (in atomic units)

$$h_{\mu\nu} = \left\langle \chi_\mu \left| -\frac{1}{2}\nabla^2 - \sum_K \frac{Z_K}{|\mathrm{R}_K - \mathrm{r}|} \right| \chi_\nu \right\rangle, \tag{10}$$

and $\mathbf{G}(\mathbf{D})$ represents the two-electron interaction, which in the atomic orbital basis can be written as

$$G_{\mu\nu}(\mathbf{D}) = \sum_{\rho\sigma} D_{\sigma\rho}(g_{\mu\nu\rho\sigma} - g_{\mu\sigma\rho\nu}), \tag{11}$$

with the two-electron integrals being defined as

$$g_{\mu\nu\rho\sigma} = \int\int \chi^*_\mu(\mathrm{x}_1)\chi_\nu(\mathrm{x}_1)\frac{1}{r_{12}}\chi^*_\rho(\mathrm{x}_2)\chi_\sigma(\mathrm{x}_2)d\mathrm{x}_1 d\mathrm{x}_2, \tag{12}$$

where x_i comprises a spin and a spatial coordinate. In Eqn (5), v_{nuc} is the potential energy between the nuclei and the external fields, while $\mathbf{V}$ describes the interaction between the electrons and the external fields. In the electric quadrupole approximation, the

monochromatic field–molecule interaction operator $\hat{V}(t)$ entering the Hamiltonian is given by

$$\begin{aligned}\hat{V}(t) &= -F(t)\hat{\mu} - Q(t)\,\hat{\Theta} - B(t)\,\hat{m} \\ &= -(f\ \exp(-i\omega_{\mathrm{rad}}t) + f^*\exp(i\omega_{\mathrm{rad}}t))\ \hat{\mu} \\ &\quad -(q\ \exp(-i\omega_{\mathrm{rad}}t) + q^*\exp(i\omega_{\mathrm{rad}}t))\ \hat{\Theta} \\ &\quad -(-ib\ \exp(-i\omega_{\mathrm{rad}}t) + ib^*\exp(i\omega_{\mathrm{rad}}t))\ \hat{m},\end{aligned} \tag{13}$$

in which the monochromatic electromagnetic wave is represented as an oscillating, inhomogeneous electric field and an oscillating homogeneous magnetic field, determined by corresponding complex-valued frequency component vectors f, q and b

$$f = \{f_x, f_y, f_z\}, \tag{14}$$

$$q = \{q_{xx}, q_{xy}, q_{yy}, q_{xz}, q_{yz}, q_{zz}\}, \tag{15}$$

$$b = \{b_x, b_y, b_z\}, \tag{16}$$

which we treat as perturbations (perturbation strengths), and which multiply the electric dipole-, electric quadrupole- and magnetic dipole moment operators, respectively. Since $\hat{m}$ is an imaginary operator, a factor $-i$ has been added so that b multiplies the imaginary part of $\hat{m}$, which is a real anti-Hermitian operator. This avoids having imaginary perturbed (differentiated) integrals ($\mathbf{V}^b$, etc.).

The various polarizability gradients needed for the calculation of the ROA circular intensity differences can now be obtained by straightforward differentiation of the quasi-energy gradient in Eqn 4, as described elsewhere.[35] Here we limit ourselves to presenting the final expressions for the different polarizability gradients

$$\begin{aligned}Q^{gf^*f} &= \mathrm{Tr}\{\mathbf{V}^{gf}\mathbf{D}^{f^*} + \mathbf{V}^{gf^*}\mathbf{D}^{f} + \mathbf{h}^{g}\mathbf{D}^{f^*f} \\ &\quad + \mathbf{G}^{g}(\mathbf{D}^{f^*})\mathbf{D}^{f} + \mathbf{G}^{g}(\mathbf{D})\mathbf{D}^{f^*f} - \mathbf{S}^{g}\mathbf{W}^{f^*f}\}_t,\end{aligned} \tag{17}$$

$$\begin{aligned}Q^{gf^*q} &= \mathrm{Tr}\{\mathbf{V}^{gq}\mathbf{D}^{f^*} + \mathbf{V}^{gf^*}\mathbf{D}^{q} + \mathbf{h}^{g}\mathbf{D}^{f^*q} \\ &\quad + \mathbf{G}^{g}(\mathbf{D}^{f^*})\mathbf{D}^{q} + \mathbf{G}^{g}(\mathbf{D})\mathbf{D}^{f^*q} - \mathbf{S}^{g}\mathbf{W}^{f^*q}\}_t,\end{aligned} \tag{18}$$

$$\begin{aligned}Q^{gf^*b} &= \mathrm{Tr}\{\mathbf{V}^{gb}\mathbf{D}^{f^*} + \mathbf{V}^{gf^*}\mathbf{D}^{b} + \mathbf{h}^{g}\mathbf{D}^{f^*b} \\ &\quad + \mathbf{G}^{g}(\mathbf{D}^{f^*})\mathbf{D}^{b} + \mathbf{G}^{g}(\mathbf{D})\mathbf{D}^{f^*b} - \mathbf{S}^{g}\mathbf{W}^{f^*b}\}_t.\end{aligned} \tag{19}$$

These expressions contain the first- and second-order perturbed density matrices with respect to the electric field f (or f^*), a magnetic field b and an electric field gradient q, respectively. These perturbed density matrices are determined using the linearly scaling response solver of Coriani *et al*.[39]

It is worth noticing that in contrast to other analytic implementations of ROA[31–33], the equations above utilize the so-called $n + 1$ rule instead of the $2n + 1$ rule. In this way, we avoid having to solve equations for a perturbed density matrix for each displacement of the nuclei (of which there are three times the number of the nuclei), limiting the number of perturbed density matrices that need to be determined to 45, independent of the size of the molecule. These 45 densities are 12 first-order perturbed density matrices (3 for the dipole moment operator, 3 for the magnetic dipole moment and 6 for the quadrupole operator using the symmetry of the operator), and 33 determined by means of second-order equations (6 second-order in the electric fields, 9 mixed electric–magnetic dipole second-order and 18 mixed electric dipole–electric quadrupole perturbed density matrices).

For the solvent calculations we have used the extension of integral-equation formalism polarizable continuum model IEF-PCM[40–42] for the calculation of ROA circular intensity differences as described by Pecul *et al*.[24] In this approach, the different electronic polarizabilities are calculated analytically, but the geometrical derivatives of the polarizabilities are obtained by finite displacements of the nuclear positions. Local field effects have not been included, as these can be expected to be of minor importance for properties involving mixed hyperpolarizabilities.[24] Even though the implementation in Ref. [24] allows London orbitals to be utilized, we will only report the numbers obtained without London orbitals in order to facilitate the discussion of the solvent effects, since our analytical approach used for the gas-phase calculations has not yet been extended to allow for the use of London orbitals, even though the formalism has been described in detail in Ref. [29]. We have verified that the difference between London and non-London results is small.

The structures of anionic, cationic and zwitterionic forms of hydroxyproline have been optimized at the DFT(B3LYP)/aug-cc-pVDZ level using the Gaussian03[43] program. Gaussian03 was also used to obtain the vibrational Hessian. The PCM in its integral-equation formalism (IEF-PCM)[40,44–46] with standard van der Waals radii for functional groups (as default in Gaussian03[43]) and the α factor set to 1.2 has been used to simulate the aqueous environment. In the case of the anionic and cationic structures, also gas-phase-like optimizations (of the isolated molecules) have been carried out. The optical tensors, for the isolated molecules and in the PCM-simulated aqueous environment, have been calculated using a local version of DALTON.[47] The ROA intensities have been calculated at the Hartree–Fock level of theory using the aug-cc-pVDZ basis set.

The vibrational modes have been analyzed in terms of potential energy distribution (PED) using the VEDA program[48] and visualized by means of PyVib2.[49,50] The presented spectra have been simulated by representing each ROA band as a Lorentz-shaped curve with a half-width of 5 cm^{-1}.

Experimental details

Trans-4-hydroxyproline-L-proline was purchased from Fluka. The solutions were filtered with Ultrafree-MC Amicon filters from Millipore (0.22 µm filter unit). The pH of the almost saturated solutions was adjusted with a micro-electrode. Before the measurements, the cuvette was centrifuged at 1000 g with an Eppendorf centrifuge. Scattered circular polarization (SCP) ROA backscattering spectra were taken at room temperature, with the exciting wavelength of 532 nm and a depolarized incident beam.[3] The resolution was 7 cm^{-1} and the sample size was 35 µl. Seven-point third-order Savitzky–Golay smoothing was applied.

Results and Discussion

Molecular structures

The starting structures for the geometry optimizations have been selected partly on the basis of the gas-phase conformations of neutral 4(*R*)-hydroxyproline[51] and cationic and anionic proline,[52] and partly on the basis of the proline structures obtained in Ref. [52]. The optimized minimum structures (as obtained by means of PCM) are shown in Figs 1,2 and 3, while the energy is tabulated in Tables 1, 2, and 3, respectively. In all cases, the conformations are listed according to increasing energy. For anionic and cationic forms of hydroxyproline, we decided to perform the calculations also for gas-phase isolated ions, to allow for a comparison with PCM results. No gas-phase data are listed

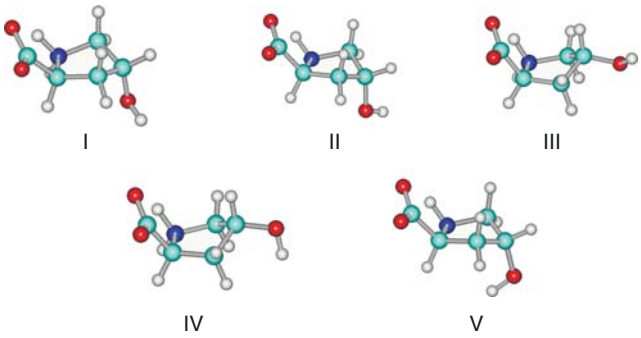

Figure 1. The predicted low-energy conformers of zwitterion 4(*R*)-hydroxyproline.

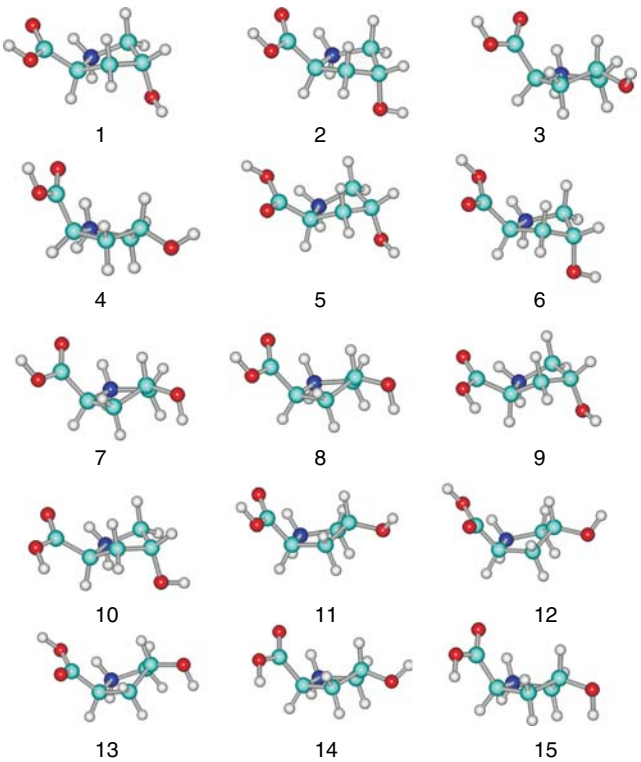

Figure 2. The predicted low-energy conformers of cationic 4(*R*)-hydroxyproline.

for hydroxyproline in the zwitterionic form, since zwitterionic structures are unstable without an aqueous environment.

The two lowest zwitterionic structures (Fig. 1), **I** and **II**, both have the *endo* conformation of the ring and differ only in the arrangement of the hydroxyl group. This is in agreement with the findings of Pecul *et al*.[52] for neutral and ionic proline and with Kapitan *et al*.[37] for the zwitterion form, where the forms of proline lowest in energy has *endo* conformation of the pyrrolidine ring (ring down-puckered with respect to the carboxyl group). The next two structures, significantly higher in energy (Table 1), have the *exo* form of the ring (ring up-puckered with respect to the carboxyl group). All low-lying structures under consideration have an internal hydrogen bond between the $-NH_2^+$ and COO^- groups. We have omitted the neutral forms of 4(*R*)-hydroxyproline in our subsequent calculations. This omission should not introduce large errors in the following calculations of the ROA spectra, since

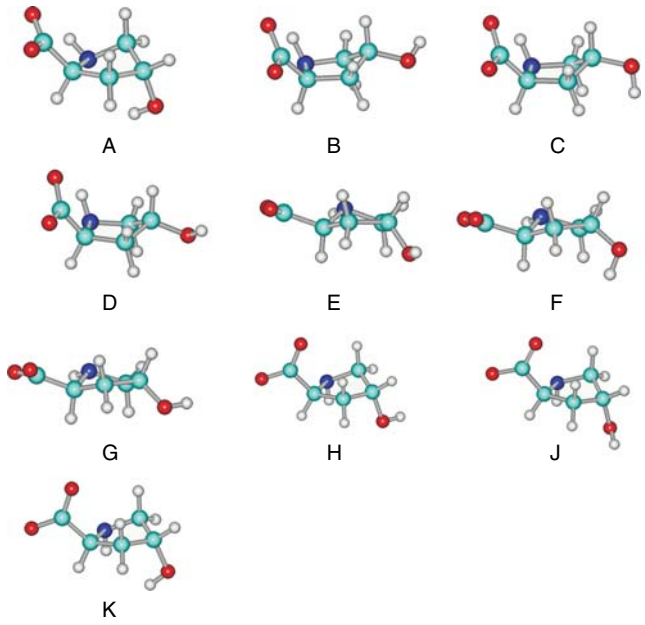

Figure 3. The predicted low-energy conformers of anionic 4(*R*)-hydroxyproline.

there is a sizable energy gap between the most stable zwitterionic form and the most stable neutral form in aqueous environment.

The cationic form has two conformations with low energy, again both with the *endo* form of the ring (Fig. 2). As for the anionic proline, although to a lesser extent, the energy gaps between different conformers are lowered when geometry optimization is carried out using PCM, as shown in Table 2. It is worth noting that there are more minima in the dielectric environment than for the isolated molecules, since for the latter some of them converge to the same structures.

In the case of the anionic form of 4-(*R*)-hydroxyproline, there is a large energy gap between the four conformations which are lowest in energy and the remaining structures (Table 3). The lowest structure has the *endo* form of the ring (Fig. 3), while the next three, differing only in the conformation of the hydroxyl group, have the *exo* form of the ring. When the geometry optimization is carried out using the PCM model, the four lowest lying structures are very close in energy (the energy gap between the first and fourth structure is less than 1 kJ/mol). However, we emphasize that the well-known problems of DFT in the description of diffuse states (including anionic species, see for example Ref. [52]) make the results obtained for anionic hydroxyproline less reliable than for the other forms. This is true not only for the geometries but also for the ROA intensities as discussed below.

ROA spectra

We will discuss and compare the calculated and experimental ROA spectra of 4(*R*)-hydroxyproline. Since the comparison with experiment is possible only for wavenumbers lower than 1900 cm^{-1}, the spectra are shown only up to this wavenumber. Arbitrary units are used for the ROA intensities. If not specifically noted, the vibrations described are for the first conformer drawn in Figs 1–3, corresponding to the conformer of lowest energy of the zwitterionic, cationic and anionic forms of 4(*R*)-hydroxyproline, respectively. The averaged spectra have been calculated using Maxwell–Boltzmann distributions, employing relative energies at

Table 1. The energy of zwitterion hydroxyproline relative to the lowest conformer, in kJ/mol. PCM results. D_0 contains zero-point vibrational correction

	D_e	D_0
I	0.0	0.0
II	0.6	0.6
III	5.1	4.5
IV	7.4	7.4
V	10.4	9.2

Table 2. The energy of cationic hydroxyproline relative to the lowest conformer, in kJ/mol. D_0 contains zero-point vibrational correction

	Gas-phase			PCM	
	D_e	D_0		D_e	D_0
1	0.0	0.0	**1**	0.0	0.0
2	1.8	1.3	**2**	0.4	0.4
4	17.8	16.6	**3**	10.4	10.9
5	19.5	19.0	**4**	10.4	10.1
6	21.7	20.7	**5**	11.7	11.2
8	27.0	26.5	**6**	12.1	11.8
9	31.9	30.6	**7**	14.0	13.6
10	32.6	31.1	**8**	14.0	14.5
11	38.1	36.7	**9**	17.2	16.7
3	47.5	47.1	**10**	17.7	17.2
14	47.8	45.6	**11**	23.0	23.5
13	49.2	47.9	**12**	23.2	22.3
15	58.3	56.9	**13**	26.9	26.6
–	–	–	**14**	27.0	26.6
–	–	–	**15**	30.8	31.3

Table 3. The energy of anionic hydroxyproline relative to the lowest conformer, in kJ/mol. D_0 contains zero-point vibrational correction

	Gas-phase			PCM	
	D_e	D_0		D_e	D_0
A	0.0	0.0	**A**	0.0	0.0
C	8.3	6.9	**B**	0.5	0.6
D	9.5	8.2	**C**	0.6	1.0
B	12.1	10.8	**D**	0.7	0.7
F	28.2	25.2	**E**	11.3	10.2
E	32.1	29.0	**F**	12.0	11.0
G	35.7	32.4	**G**	12.5	11.0
J	39.5	37.7	**H**	13.3	13.3
H	41.2	39.9	**J**	13.5	13.4
–	–	–	**K**	16.7	16.1

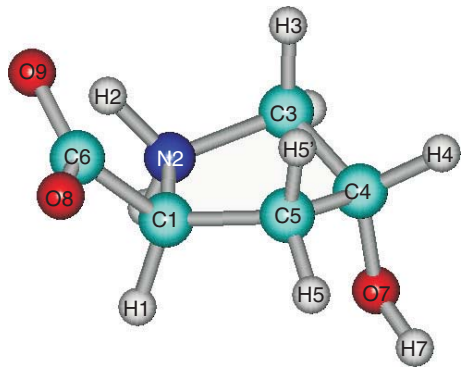

Figure 4. Atom numbering in 4(*R*)-hydroxyproline.

0 K (including zero-point vibrational energies). The appearance of the calculated spectra is not changed when free energies evaluated at room temperature are used instead. The experimental peaks are assigned to specific vibrational modes on the basis of comparison with theoretical predictions and PED analysis. The atom numbering used in the following analysis is shown in Fig. 4.

Figure 5 contains the experimental Raman and ROA spectra of 4(*R*)-hydroxyproline collected for three pH values. The effect of pH change on them is not very large: the largest change is the additional band at 1736 cm^{-1} (visible only in the Raman spectrum) in the spectrum taken at pH = 1, corresponding to the stretching of the carboxyl group coupled with the bending vibration of the acidic proton (see below). This spectrum also lacks the band at 1430 cm^{-1}, present in those taken at pH = 6 and pH = 10, and the sign of the ROA band at 1380 cm^{-1} is reversed with respect to the other two spectra. It should be mentioned at this point that the effects of pH may be exaggerated in the theoretical spectra, since we assume there are only cations in the acidic solution and only anions in the basic one, while the actual composition of the solution is more complicated.

Zwitterionic form ($NH_2^+CHRCOO^-$)

The calculated ROA spectra of the 4(*R*)-hydroxyproline zwitterion are shown in Fig. 6, the uppermost spectrum obtained by including PCM only for the geometry optimization and force field (PCM/gas) and the one in the middle with the optical tensors also calculated using PCM (PCM/PCM). The experimental spectrum collected at pH = 6, where the zwitterionic conformations are dominant, is shown below for comparison. The calculated spectra originate predominantly (88%) from the two lowest zwitterionic conformations (**I** and **II**).

The most striking feature of the theoretically obtained spectra is that treatment of the solvent by means of PCM increases the ROA intensities of the ν(C–H) stretching vibrations (with large ROA intensity, not shown in Fig. 6) by one order of magnitude. ROA intensities of the other vibrations are also increased (in terms of their absolute value) when placing the molecule in the dielectric medium, but to a lesser extent. However, the instances where the use of PCM for the optical tensors change the sign of the ROA intensity of a vibration are rare.

Rather surprisingly, the calculated spectrum is closer to experiment when PCM is used only in the geometry and force field calculations (the PCM/gas spectrum), especially in the region below 1400 cm^{-1}, than when PCM is used also for the calculations of optical tensors. Below, we ascribe the most active ROA bands to the specific vibrations on the basis of a PED analysis.

The theoretically predicted $\nu(COO^-)$ antisymmetric stretching vibration with some NH_2 bending has a wavenumber of 1674 cm^{-1} in both of the leading conformations (to be compared with the experimentally observed wavenumber of 1645 cm^{-1}), and a negative ROA activity (strong in conformer **I**, weak in conformer **II**). Close to it (1596 cm^{-1} in the theoretical spectrum, 1582 cm^{-1} in the experimental spectrum) there is a band corresponding

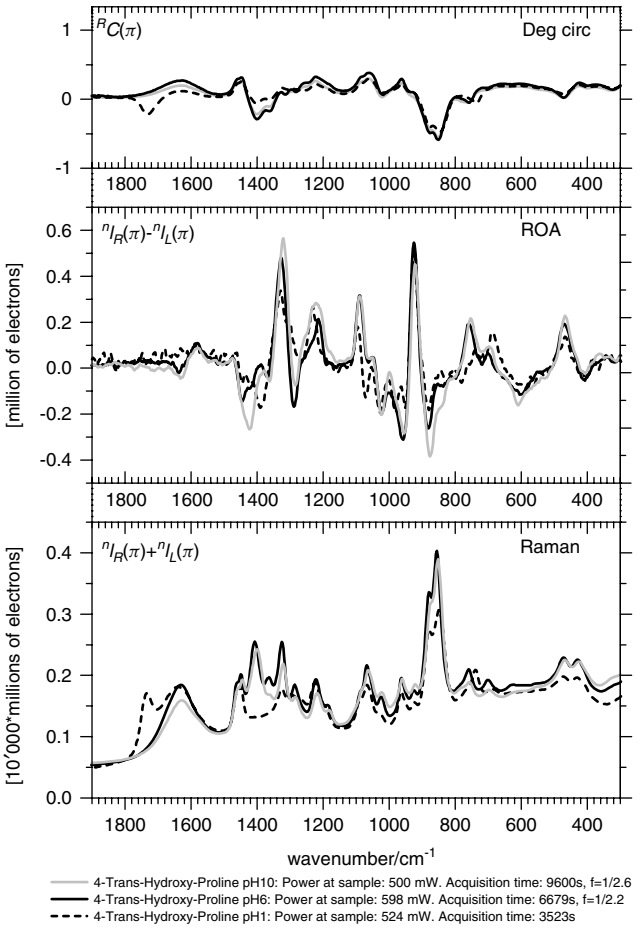

Figure 5. The experimental ROA, Raman and degree of circularity spectra of 4(*R*)-hydroxyproline (100 mg/ml) collected in H_2O at pH = 1, 6 and 10.

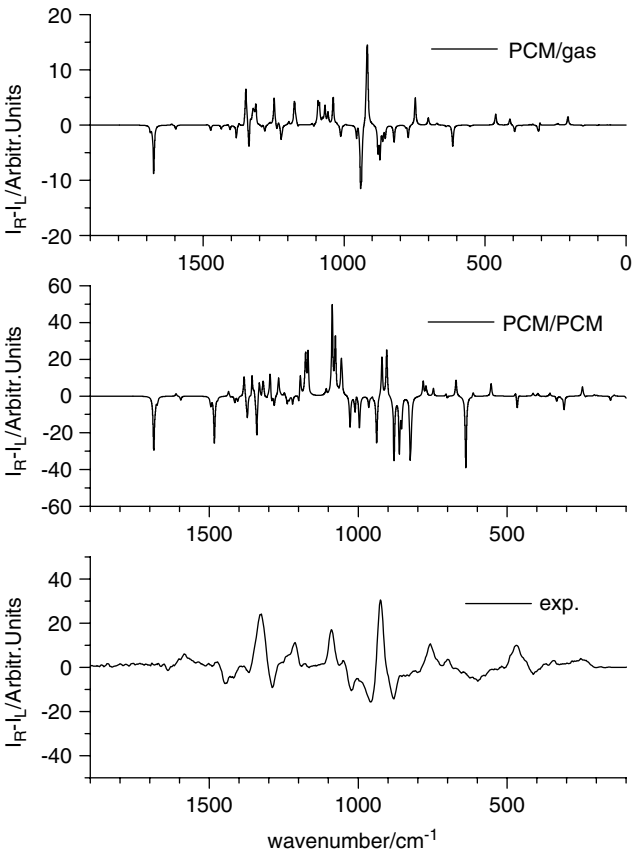

Figure 6. The calculated Boltzman-averaged ROA of the zwitterion 4(*R*)-hydroxyproline (in arbitrary units) and the experimental ROA spectrum of 4(*R*)-hydroxyproline (less than 100 mg/ml) collected at pH = 6, acquisition time: 5679 s, power at sample 598 mW.

to the $\delta(NH_2)$ bending vibration with a small contribution from the $\nu(COO^-)$ antisymmetric stretching vibration with a very weak ROA intensity, which disappears almost completely in D_2O (see Fig. S1 of the Supporting Information). The contribution of the bending vibration is larger here than in the one at 1645 cm^{-1}. The calculated ROA intensity of ν(C–O) at 1674 cm^{-1} is overestimated in comparison to experiment, whereas that of $\delta(NH_2)$ at 1596 cm^{-1} is somewhat underestimated. The ROA intensity of $\delta(NH_2)$ is positive in experiment, whereas the calculations give a positive value only for one conformer and only when PCM is used for both force field and optical tensors. The weak negative experimental band at 1491 cm^{-1} can be identified as an in-phase $\delta(CH_2)$ scissoring mode of large amplitude on both C5 and C3. It is theoretically predicted at 1484 cm^{-1}, also with a negative ROA intensity, in the PCM/PCM spectrum. The in-phase scissoring mode is followed by an out-of-phase mode, giving a weak positive peak at 1475 cm^{-1}, to which corresponds a medium-strong negative band predicted in the theoretical spectrum at 1472 cm^{-1}. The region from 1473 to 1360 cm^{-1} shows strong pH dependence (Fig. 5). The most negative experimental peak, at 1449 cm^{-1}, is present at all three pH values. Surprisingly, it does not have a corresponding theoretical peak for neither conformer I nor II. The experimental negative peak of medium intensity at 1412 cm^{-1} (weakly negative at 1404 cm^{-1} in the theoretical spectrum) corresponds primarily to a stretching of the C4–C5 bond coupled with strong, in-phase deformations of the hydrogens on C4 and O7. This vibration is of comparable experimental intensity at pH = 1, more negative at pH = 10 and also more negative for the ROA spectrum of proline at this wavenumber (see Fig. S1 of Supporting Information).

The band at 1328 cm^{-1} in the experimental spectrum with a very large positive ROA activity is probably an overlap of the theoretical peaks at 1332, 1324 and 1318 cm^{-1} (as both the PCM/gas and PCM/PCM spectra indicate). The vibration at 1332 cm^{-1} contains contributions from the $\delta(NH_2)$ bending, a $\nu(COO^-)$ symmetric stretch, a weak C3H_2 twisting and a C5H_2 wagging, a C6–C1 and C1–C5 antisymmetric stretch and a deformation of the hydrogen on the two asymmetric carbons C*1, C*4 and on O7 (the O7–H7 deformation is weak). Deformations of the C–H bonds on asymmetric carbons very often give strong ROA signals. Such a deformation is also present at 1324 cm^{-1}, but the movements of the two hydrogens are in a plane situated at about 90° to the plane which contains the deformations of the hydrogens at 1332 cm^{-1}. The direction of these C*H deformations is identical at 1332 and 1318 cm^{-1}. The vibration at 1324 cm^{-1} shows a stronger deformation of H7 than the vibration at 1332 cm^{-1}, without a C1–C6 but with a C4–C5 stretching component.

The origin of the next experimental negative ROA band at 1289 cm^{-1} is less certain: it is probably present as two peaks in the PCM/PCM spectrum and as one peak in the PCM/gas spectrum, and it may have (in conformer I) a contribution from the deformation of the hydrogen on the C*1, C*4 and O7 atoms, some stretching of the C1–C6 bond, some NH(H) deformation and some wagging of the C5–H2 moieties. The positive peak at 1212 cm^{-1} (negative

at 1220 cm^{-1} in the theoretical spectrum) represents mostly the twisting of $C3H_2$, $C5H_2$ and NH_2 moieties with some deformation of the hydrogen on the asymmetric C*1 and C*4 carbon atoms. This peak disappears almost completely in the D_2O spectrum (see Fig. S1 of Supporting Information).

The 'pure' δ(H1–C1–C6) bending vibration has positive ROA intensity as predicted by the calculations (wavenumbers of 1173 or 1176 cm^{-1}, depending on the conformer), and it may correspond to the positive experimental ROA peak of very weak intensity at 1191 cm^{-1}. The negative ROA intensity of proline at this wavenumber is stronger (see Supporting Information). The next experimental peak of medium to strong positive intensity is at 1090 cm^{-1}; it probably corresponds to the strongest positive theoretical peak at 1087 cm^{-1} in the PCM/PCM spectrum: a stretching of the C4–O7 and C1–C5 bond simultaneously with a twisting of the $C3H_2$, $C5H_2$ and NH_2 groups. The small experimental peaks at 1067 cm^{-1} (negative) and 1051 cm^{-1} (positive) represent stretching of the pyrrolidine ring and of the C4–O7 bond.

The negative peak of medium intensity, present for all pH values at 1023 cm^{-1}, does not have a corresponding theoretical vibration in conformer **I** and **II**. The next sizable ROA band in the experimental spectrum is that at 1010 cm^{-1} (weakly positive). A comparison with the theoretical spectra allows us to identify it as an asymmetric stretching vibration of the C1–N2–C3 ring fragment. The strongest negative experimental peak at 958 cm^{-1} can be related to the theoretical negative one at 955 cm^{-1}, being a partial ring breathing without movement of the N2–C1 bond. The very strong positive ROA band at 925 cm^{-1} in the experimental spectrum covers two distinct vibrations in the PCM/PCM spectrum, which represents the experimental spectrum better than the PCM/gas spectrum in the region between 958 and 880 cm^{-1}. The first band (938 cm^{-1}) is a stretching of the N2–C1, C1–C5, C1–C6 bonds with the C3 atom immobile. The second is composed of two antisymmetric stretchings of the N2–C3 and C5–C4 bonds. The next negative band at a wavenumber of 880 cm^{-1}, in good agreement with the theoretical spectrum, is a C1–C5 bond stretching (853 cm^{-1}) and a C3–C4 bond stretching (879 cm^{-1}), both vibrations coupled with torsional movements of the atoms in the ring.

The experimental positive ROA band at 757 cm^{-1} could be described as an out-of-plane bending mode of the COO^- group predicted at 747 cm^{-1} in the theoretical spectrum (or an H1C1C6 rocking mode), according to the results obtained with PCM used only for the geometry optimization and force field calculations, whereas the small positive ROA band at 700 cm^{-1} seems to come from the bending of O8C1C4 and of a torsional movement of the N2–C3 and N2–C1 bonds, N2 moving alternatively in and out the ring.

The medium-weak positive peak at 469 cm^{-1} corresponds to the theoretical δ(C6C1O8) bending mode at 462 cm^{-1}, with a deformation of O7 from the C4–O7 bond in phase with the bending; this vibration is also present at pH = 10 at 466 cm^{-1} and at pH = 1 at 440 cm^{-1}. In this motion, all atoms of the pyrrolidine ring move as a block, carried by the bending motion; the peak is negative in the PCM/PCM spectrum and positive in the PCM/gas spectrum. The experimental peak at 413 cm^{-1} (negative) could correspond to the theoretical peak at 412 cm^{-1}, which is principally a rocking of $C3H_2$ and $C5H_2$ with deformation of the hydrogen in O7–H7. The strong deformation of the hydrogen on O7, almost parallel to the ring, predicted theoretically at 331 cm^{-1} (weak negative in the PCM/PCM spectrum and weak-positive in the PCM/gas spectrum), is present at 347 cm^{-1} as a weak positive peak in the experimental spectrum. Summarizing, the largest positive and negative ROA intensities are exhibited by the deformation of the hydrogen atom on the asymmetric C*1 and C*4 atoms and the stretching vibrations of the five-membered ring of hydroxyproline.

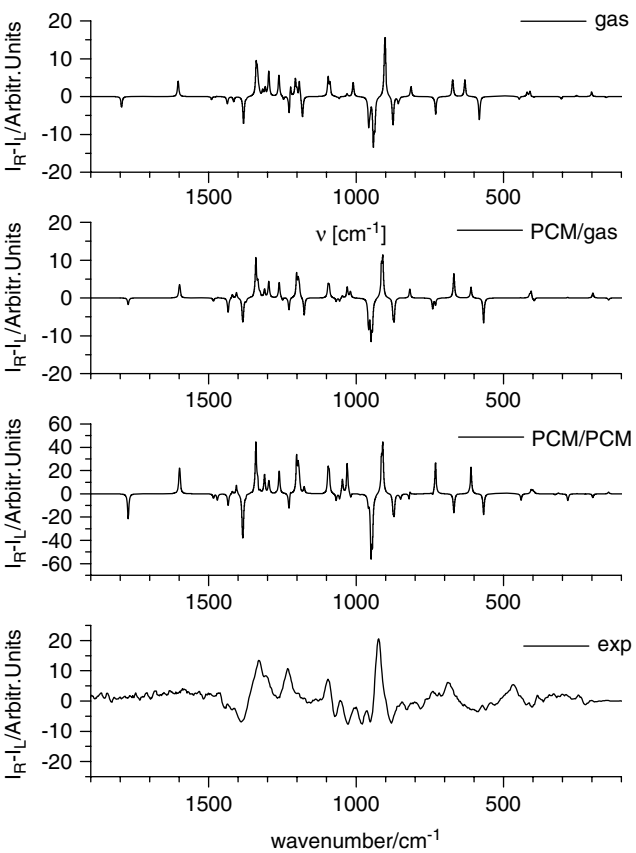

Figure 7. The calculated Boltzman-averaged ROA of the cationic 4(*R*)-hydroxyproline (in arbitrary units) and the experimental ROA spectrum of 4(*R*)-hydroxyproline (100 mg/ml) collected at pH = 1, acquisition time: 3523 s, power at sample 524 mW.

As far as the conventional Raman spectrum is concerned, the agreement of the calculated and experimental spectrum (Fig. S2 in Supporting Information) is much better than in the case of ROA, especially when PCM is used only for geometry optimization and force field calculations. However, using PCM also for dipole polarizability tensor increases Raman intensities by one order of magnitude, and, similar to ROA, worsens the agreement with experiment.

Cationic form (NH_2^+CHRCOOH)

The calculated ROA spectra of the cationic form of hydroxyproline and the experimental ROA spectrum collected for pH = 1 are shown in Fig. 7. The atom numbering used in this section is as in Fig. 4, and the proton H8 is defined to be attached to O8. The calculations have been carried out for an isolated cation (the uppermost graph, denoted 'gas'), employing PCM for geometry optimization and force field only (the second graph, denoted 'PCM/gas'), and employing PCM for geometry optimization, force field and optical tensors (the third graph, denoted 'PCM/PCM'). In the case of the cation, two conformations (1 and 2) dominate the averaged ROA spectrum. Unlike in the case of the zwitterion, it is difficult to say which of the PCM/gas and PCM/PCM spectra is in better agreement with experiment.

When the experimental spectrum is analyzed starting from the highest wavenumber, one can observe that the ν(C═O) stretching vibration associated with an O8–H8 deformation and some NH_2 bending motions, predicted to have small negative ROA intensity in the PCM/gas approach and much larger in the PCM/PCM approach at 1790 cm^{-1}, is not visible at all in the experimental ROA spectrum. However, it is present at 1736 cm^{-1} in the degree of circularity and Raman spectrum (see Fig. 5). The experimental, weak, positive ROA peak at 1589 cm^{-1} is a strong $\delta(NH_2)$ bending mode present at 1600 cm^{-1} in the PCM/gas and PCM/PCM spectra, identical as at pH = 6. The weak negative experimental band centered at 1488 cm^{-1} can be identified as an in-phase $\delta(CH_2)$ scissoring mode of hydrogen atoms on both C5 and C3. It is theoretically predicted at 1483 cm^{-1}, with a weak negative ROA intensity in the PCM/PCM spectrum. The in-phase scissoring mode is followed by an out-of-phase mode of weak positive intensity at 1470 cm^{-1} in the experimental spectrum, to which corresponds a weak negative band predicted at the same wavenumber.

The theoretical PCM/PCM spectrum shows good agreement with experiment as far as the next discernible ROA bands from 1460 to 1350 cm^{-1} in the experimental spectrum are concerned, except for the sign of the theoretical peak at 1419 cm^{-1}. The negative peak at 1433 cm^{-1} originates from a combination of an antisymmetric stretch of O8–C6–C*1 with an H8–O8–C1 bending, deformations of the hydrogens on C*1 and C*4 (small contribution), an NH_2 twisting and a $C3H_2$ wagging (small contribution). The negative peak of medium-weak intensity at 1426 cm^{-1} in the experimental spectrum probably corresponds to a theoretical peak at 1419 cm^{-1}, which is a combination of ν(C3–C4) stretching, an in-phase deformation of H7 and H4, an in-phase wagging of NH_2 and $C3H_2$ and a rocking of $C5H_2$. The peak at 1382 cm^{-1}, the most negative peak of all of these, does not have any contribution from the COO^- symmetric stretch found in the zwitterionic and anionic forms, as the group is protonated. In the cationic form, the peak at this wavenumber corresponds to an NH_2 wagging, a $C3H_2$ twisting and deformation of the hydrogen atoms bound to O8, O7 (small contribution), C*1 and C*4.

The large positive experimental ROA band which culminates at 1325 cm^{-1} seems to contain three theoretically calculated peaks at about 1340, 1331 and 1310 cm^{-1} both in the PCM/PCM and PCM/gas spectra. All of these bands result from a strong deformation of the hydrogens on both chiral centers C*1 and C*4. The theoretical vibration at 1340 cm^{-1} for conformer 1 corresponds additionally to a twisting of $C3H_2$, a wagging of $C5H_2$, a C1–C5 stretching and a deformation of the hydrogens on O8 and O7. The vibration at 1310 cm^{-1} stems from an antisymmetric stretching of C4–C5 and C1–C5, a rocking of $C3H_2$, a twisting of $C5H_2$ and NH_2 (small contribution) and a weak deformation of the hydrogens on O8 and O7. The vibration at 1331 cm^{-1} is an H8–O8 deformation with a C6–O8 stretching, a wagging of $C3H_2$ and $C5H_2$ and a weak rocking of NH_2. All vibrations from 1340 to 1250 cm^{-1} are pH-dependent, with particularly strong dependence of those visible in the experimental spectrum from 1310 to 1250 cm^{-1} (Fig. 5).

The experimental pH-specific shoulder at 1296 cm^{-1} corresponds to a theoretical positive peak of similar intensity at the same wavenumber. It contains components from a $C5H_2$ wagging, a C4–C5 stretching, an in-phase displacement of one hydrogen on NH_2 and of another on the opposite side of the ring on $C3H_2$, and deformations of the hydrogen atoms in the C*1–H, C*4–H and O8–H8 bonds. The experimentally determined peak of very low intensity at 1266 cm^{-1} may correspond to a theoretically predicted positive peak at 1260 cm^{-1}. It originates from a combination of an NH_2 twisting, a $C3H_2$ rocking and a deformation of the hydrogens on C*1 (in phase with C5H5H5′), C*4, O7 and O8 (small contribution).

The next positive ROA band (the third most positive) at 1232 cm^{-1} seems to correspond to the negative theoretical peak at 1227 cm^{-1}. It has contributions from H5–C5–C1 and H7–O7–C4 bending modes $C3H_2$ and $C5H_2$, antisymmetric twisting and a deformation of the hydrogen on NH(H) and O8–H8. Almost no vibrations are present in the region between 1200 and 1100 cm^{-1}. The theoretical peaks of medium-strong intensity at about 1200 cm^{-1} are very weak in the experimental spectrum. The positive peak present experimentally at 1096 cm^{-1} and predicted theoretically at 1087 cm^{-1} seems to come from the ν(C4–O7) stretching mode and the stretching of the C1–C5 bond. The next experimental negative peak at 1073 cm^{-1}, of weak to medium intensity, could correspond to the weak negative theoretical peak at 1069 cm^{-1}, which is principally a stretching of the C5–C1, C5–C4, N2–C4 and C4–O7 bonds with a rocking of $C3H_2$. The quite large theoretical negative peak at 1028 cm^{-1} could correspond to the positive experimental peak at 1030 cm^{-1} with a wrong sign assignment to this peak, which is of medium intensity in the PCM/PCM spectrum and of weak intensity in the PCM/gas spectrum. The peak at 1030 cm^{-1} is an antisymmetric stretching of the N2–C1–C5 group, a C3–C4 stretch and a rocking of the $C5H_2$, $C3H_2$ and NH_2 groups, with deformation of the hydrogen on C*4 and C*1. The negative experimental peak at 984 cm^{-1} does not have a theoretical counterpart in conformers 1 and 2.

The most significant difference between theory and experiment is the lack of strong negative experimental ROA bands at approximately 960–949 cm^{-1}, but there is a weak negative peak present at 952 cm^{-1} in the theoretical spectrum, originating from the pyrrolidine ring breathing with N being motionless. The strongest positive experimental ROA band at 923 cm^{-1} probably includes the two strong theoretical peaks (positive at 909 cm^{-1}, an alternative stretching of the N2–C3 and C4–C5 bonds and negative at 949 cm^{-1}, and a stretching of the C1–C6, C4–C3, C4–O7 and C1–N2 bonds). The pyrrolidine ring breathing has a negative signal of medium intensity at 880 cm^{-1} in the experimental spectrum and at 870 cm^{-1} in the theoretical one.

The next region, from 860 to 650 cm^{-1}, shows a distinct experimental profile for the cationic form of *trans*-4-hydroxy-L-proline compared to the anionic and zwitterionic forms. For example, the negative peak at 856 cm^{-1} in the PCM/PCM spectrum may correspond to the negative shoulder at 856 cm^{-1} in the experimental spectrum, and stems from a ring breathing with C4–O7 stretching, NH_2, $C5H_2$ and $C3H_2$ rocking and a slight deformation of H8. Some CO_2 bending with O8–H8 deformation is present at 820 cm^{-1}. The positive, overestimated peak in the PCM/PCM spectrum at 740 cm^{-1}, positive at 743 cm^{-1} in the experimental spectrum, comes from a COO(H) scissoring and is also pH-dependent (Fig. 5).

The origin of the broad positive experimental ROA band at 687 cm^{-1} is uncertain: it may be a torsional vibration around the C1–C6 bond and/or the δ(OCO) scissoring mode, including an O8–H8 deformation (such is the nature of the positive PCM/PCM and negative PCM/gas peaks predicted at 668 cm^{-1}). The strong theoretical deformation of the hydroxyl group of the acid moiety, positive at 610 cm^{-1}, coupled with the COO(H) scissoring, could correspond to the weak negative peak with minimum at 596 cm^{-1} in the experimental spectrum. The overestimated negative peak at 567 cm^{-1} in the theoretical spectrum, which is principally a

strong displacement of O7–H7 without COO(H) bending but with distortions on the C6–C1 bond, could be matched by the small positive peak at 570 cm^{-1}.

We are not able to identify the positive broad band at 470 cm^{-1} since there is no substantial ROA-positive band at this wavenumber in any of the theoretical spectra. But if we look at the corresponding wavenumber at pH = 6 and pH = 10 (see Fig. 5), we have in both cases a medium-weak positive peak at 469 cm^{-1} which corresponds to the theoretical δ(C1–C6–O8) bending mode with a deformation of O7 from the C4–O7 bond in phase with the bending. The weak negative experimental peak at 414 cm^{-1} could correspond to the positive theoretical peak at 395 cm^{-1}, principally a $C5H_2$ rocking.

Similar to the case of the zwitterion, the conventional Raman spectrum intensities are in better agreement with experiment than the ROA intensities (see Fig. S3 in Supporting Information). Again, it seems better to use PCM for geometry optimization and force field calculations, but not for calculation of optical tensors.

Anionic form ($NHCHRCOO^-$)

Figure 8 presents the calculated Boltzman-averaged ROA spectrum of the anionic form of 4(*R*)-hydroxyproline (in arbitrary units). As for the cation, the theoretical results have been obtained for an isolated anion (upper graph, denoted 'gas'), an anion with force field and Boltzman factors obtained using PCM and optical tensors calculated for an isolated anion (PCM/gas), and an anion in a PCM cavity simulating the aqueous environment (PCM/PCM).

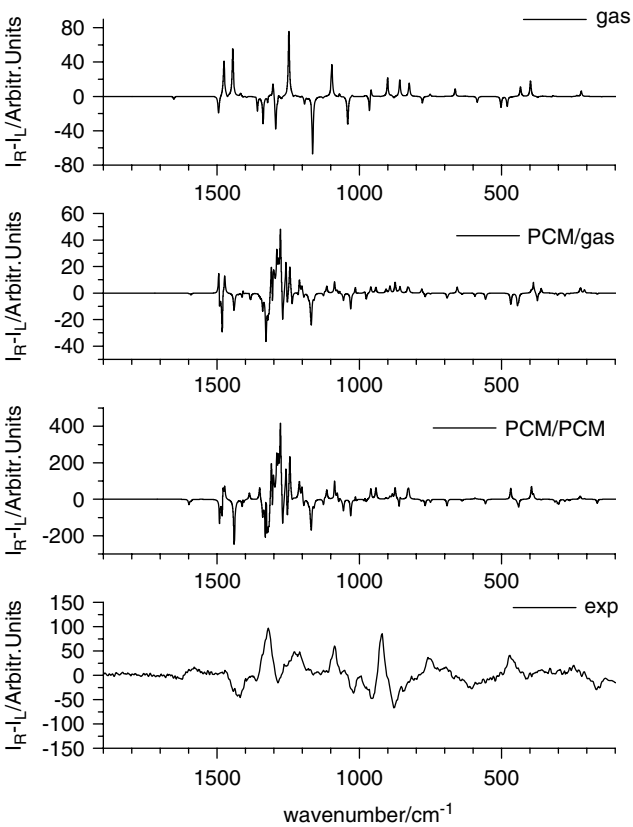

Figure 8. The calculated Boltzman-averaged ROA of the anionic 4(*R*)-hydroxyproline (in arbitrary units) and the experimental ROA spectrum of 4(*R*)-hydroxyproline (100 mg/ml) collected at pH = 10, acquisition time: 3993 s, power at sample 500 mW.

In the case of the isolated anion, the spectrum originates in 90% from conformer **A**, with an *endo* conformation of the pyrrolidine ring (the most stable by far, as shown in Table 3). In the aqueous environment, there are four low-lying conformers (**A**, **B**, **C**, **D**) contributing to a comparable degree to the averaged spectrum. **B**, **C** and **D** are in the *exo* conformation, and all four conformers have the acid moiety in the same orientation toward the NH group, allowing for an internal hydrogen bond. These specific positions of COO^- and NH are not found in conformers **E**, **F** or **G**. Calculating the optical tensors for the anion placed in a dielectric environment increases the ROA intensities by nearly one order of magnitude (graph 'PCM/PCM' in Fig. 8), and the change is similar for all vibrations. However, the relative intensities in the most interesting region of 900–1500 cm^{-1} remain approximately the same as in the case when only force field and Boltzman factors have been calculated using PCM (graph 'PCM/gas' in Fig. 8).

The experimental signal with a small positive ROA intensity at 1581 cm^{-1} originates from an antisymmetric stretching vibration of the COO^- group. It has a similar wavenumber in all four low-lying conformers (from 1591 to 1600 cm^{-1}), but its ROA intensity is positive in the **B** conformer and negative in the remaining three conformers. At the corresponding wavenumbers we have at pH = 6 and pH = 1 (see Fig. 5) an NH_2 bending motion. The antisymmetric stretching of the COO^- group of the zwitterionic form contributes primarily to the band at 1645 cm^{-1}.

The two bands just below 1500 cm^{-1} originate from an in-phase (theoretically at 1492 cm^{-1}, experimentally at 1505 cm^{-1}) followed by an out-of-phase (theoretically and experimentally at 1473 cm^{-1}) scissoring vibration of the $C5H_2$ and $C3H_2$ groups. These two vibrations have opposite signs for the ROA intensity in all four low-lying conformers, and those signs differ among the conformers. This, coupled with the substantial ROA activity of these vibrations, creates a complicated signal in the Boltzmann-averaged spectrum. The negative experimental band at 1440 cm^{-1} is primarily a δ(HNC) bending vibration, a weak deformation of the hydrogen on C*1, C*4 and O7 and an in-phase $C3H_2$ and $C5H_2$ wagging (small contribution). It is negative in three of the low-lying conformers, and positive only for **A**. In the weighted averaged spectrum it is negative in both the PCM/PCM and PCM/gas spectra. The next medium-strong negative peak at 1419 cm^{-1} is present in the experimental spectrum only at pH = 10 (Fig. 5). The nearest theoretical positive peak is that at 1406 cm^{-1}, of weak intensity, an out-of-phase deformation of the hydrogens attached to O7 and C4, with some NH vibrations and CH_2 wagging. The experimental peak we see from 1360 to 1380 cm^{-1} is positive at pH = 6 and pH = 10 and negative at pH = 1. It corresponds in the theoretical spectrum of the anion to a COO^- symmetric stretch coupled to a C1–C4 stretching at 1385 cm^{-1}.

The largest positive band in the experimental spectrum extends from 1364 to 1256 cm^{-1} with the maximum at 1320 cm^{-1} and shoulders at 1342 and 1331 cm^{-1}. It corresponds to the multitude of negative and positive theoretical bands present in the PCM/PCM and PCM/gas spectra. The theoretical peak at 1339 cm^{-1} has a large contribution from a $C3H_2$ wagging, a stretching of the C1–N and N2–C3 bonds, an NH deformation and a deformation of the hydrogens on C*1 and C*4. The shoulder at 1331 cm^{-1} corresponds to the strongest negative theoretical peak and has no theoretical correspondence when looking solely at the spectrum of conformer **A**. However, there is a vibration with a wavenumber 1328 cm^{-1} in conformer **C**, which is a deformation of the hydrogens on C*1 (strong), C*4 and N, a $C5H_2$ and $C3H_2$ twisting and a C4–C5 stretching. The experimental peak

culminating at 1320 cm^{-1} could correspond to a large extent to the positive theoretical peak at 1317 cm^{-1} in conformer **B**, a deformation of the hydrogens on C*1 (strong), C*4, N and O7, a $C5H_2$ and $C3H_2$ wagging and a symmetrical stretching of the N2–C1 and N2–C3 bonds. The weak negative experimental peak at 1286 cm^{-1} corresponds to the strongest positive peak in the PCM/PCM and PCM/gas spectra at 1280 cm^{-1}, a strong deformation of the hydrogen especially on C*1 and O7, but also on C*4 and N2 with some additional $C3H_2$ and $C5H_2$ wagging for conformer **B**, **C** and **D**.

The next experimental positive ROA peak of medium-strong intensity at 1229 cm^{-1} is also present at pH = 1 but almost absent at pH = 6. Looking at the theoretically simulated vibrations, we see in conformer **A** a positive peak at 1235 cm^{-1}, a C4–O7–H7 bending, an N–H, C*–4H and C*–1H deformation, a wagging of $C3H_2$ and a rocking of $C5H_2$. The experimental positive peak at 1209 cm^{-1} is present also at pH = 6 but absent at pH = 1 and thus should contain a COO^- or NH vibration. However, the nearest theoretical peak, positive at 1195 cm^{-1}, reveals a major $C3H_2$ twisting with minor NH deformation. The theoretical band at 1170 cm^{-1}, which comes from another δ(HCC) bending vibration (of the proton attached to C4), has a strongly negative ROA intensity in conformers **A** and **B**, but is very weak in the measured spectrum.

The next positive experimental peak at 1087 cm^{-1}, with intermediate intensity, corresponds to a positive theoretical peak at the same wavelength in the PCM/PCM and PCM/gas spectra, but not in the gas spectrum, and reflects a torsional mode of the ring (C1–C5 stretch, conformer A), a N2–C3 stretch (conformer B) and a deformation of the hydrogen on C*4 and on O7. This peak differs in intensity from those at pH 1 and 6, and it does not contain the NH_2, $C3H_2$ or $C5H_2$ twisting vibrations.

The subsequent broad peaks, nearly coalescent in the experimental spectrum (positive at 1051, negative at 1020 and negative at 959 cm^{-1}), probably correspond to theoretical peaks negative at 1069 cm^{-1}, negative at 1029 cm^{-1} (the peak of the largest intensity in this series) and positive at 959 cm^{-1}. The vibration at 1069 cm^{-1}, a stretching of the C3–C4 bond, is present in all three theoretical spectra (Fig. 8). The negative vibration at 1026 cm^{-1} is, at pH = 10, an in-phase stretching of the C1–N and N–C3 bonds (in conformer **A**) and a partial ring breathing; at pH = 6 and 10 the stretching is, according to the results of theoretical calculations, out of phase. The experimental peak at 959 cm^{-1} is very similar at pH = 6 and pH = 10. It stems from a ring breathing with an additional stretching of C3–C4 and C4–C5 bonds at pH = 10. There is no contribution from nitrogen movement at any of the three pH values.

The next experimental positive ROA peak culminating at 919 cm^{-1} with a shoulder at 900 cm^{-1} is almost as big as the one at 1320 cm^{-1} and it is identical at all three pH values. The nearest corresponding peak in the theoretical spectrum is a very weak, positive peak at 905 cm^{-1}, containing a C5–C4 stretching. The experimental negative peak at 879 cm^{-1} is the strongest negative signal at all wavelengths and any pH. The nearest theoretical positive peak is at 873 cm^{-1}, an antisymmetric stretching of two groups: C1–N and C1–C5–C4. The negative peak at 844 cm^{-1} is negative only at pH = 10: the nearest theoretical positive peak at 830 cm^{-1} is an OCO bending, coupled with a C6–C1 and C1–N stretching and the torsional movements of the ring. The medium intensity positive peak at 759 cm^{-1} is absent at pH = 1. The corresponding negative theoretical peak at 750 cm^{-1} in the PCM/PCM spectrum effectively contains an OCO bending and an antisymmetric motion of C1–C5 and C3–C4.

The last four major experimental peaks are positive at 694 cm^{-1} (shifted to lower wavenumbers at pH = 1), negative at 604 cm^{-1} (stronger at pH = 10), positive at 473 cm^{-1} and negative at 414 cm^{-1}; the peak at 694 cm^{-1} does not have a corresponding theoretical vibration in an anion. In a zwitterion, this vibration is a bending of O8–C1–C6 and a torsional movement of the N–C3 and N–C1 bonds. The next corresponding theoretical peaks are positive at 593 cm^{-1}, (in the PCM/gas spectrum), 466 cm^{-1} (in the PCM/PCM spectrum) and 395 cm^{-1} (in both spectra). The vibration at 593 cm^{-1} is to a large extent a C6–C1 stretching with some OCO bending; the vibration at 466 cm^{-1} is a scissoring motion of O8–C6–C1. The vibration at 395 cm^{-1} is a strong O7–H7 torsional vibration almost parallel to the ring (even stronger at 387 cm^{-1} and with an antisymmetric rocking of $C3H_2$ and $C5H_2$).

The anionic form is the only one with an NH group; we presume that the hydration of this group or the hydrogen bond between the amine and the acid group could have a large influence on the vibration of the molecule, as the anionic theoretical spectrum has the lowest correspondence with the experimental spectrum. Furthermore, as already mentioned, description of anionic species by means of DFT is problematic, and this influences the calculated geometric parameters, energetics and force field. This is also visible in the conventional Raman spectrum, shown in Fig. S4 in Supporting Information: unlike in the case of zwitterion and cationic hydroxyproline, there is little resemblance between the calculated and experimental Raman spectra of anionic 4(*R*)-hydroxyproline.

Summary and Conclusions

Vibrational ROA spectra have been measured for aqueous solutions of 4(*R*)-hydroxyproline for three different pH values. The experimental spectra collected at pH = 1, 6 and 10 show significant differences, especially in the region above 1000 cm^{-1}. We have attempted to reproduce these spectra by means of theoretical simulations. The theoretical results have been obtained for several conformations of anionic, cationic and zwitterionic forms of 4(*R*)-hydroxyproline using DFT and linear response Hartree–Fock calculations. The aqueous environment has been simulated using the IEF-PCM model.

The energetically lowest conformers have an *endo* form of the ring, as also observed for proline. The ROA spectra calculated for the zwitterionic form stem predominantly (88%) from the two lowest conformations, and this is also the case for the cation. In the case of the isolated anion, the averaged spectrum originates 90% from conformer **A** (by far the most stable, as shown also in Table 3). In the aqueous environment, there are four low-lying conformers (**A**, **B**, **C**, **D**) contributing to a similar extent to the averaged spectrum.

Whenever possible, assignment of the experimental ROA bands to individual normal modes has been carried out. It has been found that the largest ROA intensities, either negative or positive, are exhibited by stretching vibrations of the five-membered ring of 4-*trans*-(*R*)-hydroxyproline. We have tried to analyze whether there is any simple correlation between the ring conformation and the ROA intensity of the ring-stretching vibrations. However, it seems that the total ROA effect is a superposition of the influence of several structural parameters, and no such simple correlation exists.

The spectra have been modeled in two different ways: with PCM used only for the geometry optimization and force field calculations, and with PCM used also for the calculations of optical tensors. The instances where the use of PCM for optical tensors changes the sign of the ROA intensity of a vibration are rare.

Overall, using PCM only for the geometry optimization and force field calculations seems to give simulated ROA spectra which agree with the main features of the experimental spectra. The agreement is even better in the case of conventional Raman spectra, with the exception of the anionic form. The calculations of optical tensors using PCM seems to be more problematic (particularly for the zwitterionic structures) and seems actually to worsen the agreement with experiment. This may be accidental, since PCM in general is far from being a perfect tool for the simulation of the influence of an aqueous environment on the properties of hydroxyproline, as it does not account for short-range effects such as hydrogen bonds formed by the COO^-, NH_3^+ and OH groups of 4(*R*)-hydroxyproline. It would be therefore of interest to compare the results of PCM calculations with the simulations of ROA spectra by means of molecular dynamics coupled with supermolecular calculations, where hydrogen bonds would be accounted for in an explicit fashion.

Acknowledgments

The work has been financed by the Ministry of Science and Higher Education (Poland) from funds for scientific research in years 2009-2011 as project No. N N204138637 and by the Norwegian Research Council through a grant of computer time from the Supercomputing Program. KR has also received support from the Research Council of Norway through Grants 179568/V30, 162746/V00 and 177558/V30. CD received support from the Zürich University (Switzerland) through the Förderung des akademischen Nachwuchses (KFN) and the Stiefel-Zangger-Stiftung (StZ). The measurements were done at the University of Zürich on an instrument designed and constructed by W. Hug, and the authors are grateful to Prof. Hug for allowing us to use this instrument.

Supporting information

Supporting information may be found in the online version of this article.

References

[1] L. D. Barron, A. D. Buckingham, *Mol. Phys.* **1971**, *20*, 1111.
[2] L. D. Barron, M. P. Bogaard, A. D. Buckingham, *J. Am. Chem. Soc.* **1973**, *95*, 603.
[3] W. Hug, *Appl. Spectrosc.* **2003**, *57*, 1.
[4] L. D. Barron, L. Hecht, I. H. McColl, E. W. Blanch, *Mol. Phys.* **2004**, *102*, 731.
[5] E. W. Blanch, L. Hecht, L. D. Barron, *Methods* **2003**, *29*, 196.
[6] F. Zhu, N. W. Isaacs, L. Hecht, L. D. Barron, *Structure* **2005**, *13*, 1409.
[7] L. D. Barron, *Curr. Opin. Struct. Biol.* **2006**, *16*, 638.
[8] F. Zhu, G. E. Tranter, N. W. Isaacs, L. Hecht, L. D. Barron, *J. Mol. Biol.* **2006**, *363*, 19.
[9] L. D. Barron, L. Hecht, E. W. Blanch, A. F. Bell, *Prog. Biophys. Mol. Biol.* **2000**, *73*, 1.
[10] L. D. Barron, F. Zhu, L. Hecht, G. E. Tranter, N. W. Isaacs, *J. Mol. Struct.* **2007**, *834–836*, 7.
[11] P. Mukhopadhyay, G. Zuber, D. N. Beratan, *Biophys. J.* **2008**, *95*, 5574.
[12] A. F. Bell, L. Hecht, L. D. Barron, *J. Am. Chem. Soc.* **1998**, *120*, 5820.
[13] L. D. Barron, L. Hecht, A. F. Bell, *Appl. Spectrosc.* **1996**, *50*, 619.
[14] P. L. Polavarapu, *Chirality* **2008**, *20*, 664.
[15] P. L. Polavarapu, *Chem. Rec.* **2007**, *7*, 125.
[16] J. Haesler, I. Schindelholz, E. Riguet, C. Bochet, W. Hug, *Nature* **2007**, *446*, 526.
[17] P. L. Polavarapu, *J. Phys. Chem.* **1990**, *94*, 8106.
[18] R. D. Amos, *Chem. Phys. Lett.* **1982**, *87*, 23.
[19] T. Helgaker, K. Ruud, K. L. Bak, P. Jørgensen, J. Olsen, *Faraday Discuss.* **1994**, *99*, 165.
[20] K. Ruud, T. Helgaker, P. Bour, *J. Phys. Chem. A* **2002**, *106*, 7448.
[21] P. Bouř, *J. Comput. Chem.* **2001**, *22*, 426.
[22] M. Pecul, A. Rizzo, J. Leszczynski, *J. Phys. Chem. A* **2002**, *106*, 11008.
[23] M. Pecul, A. Rizzo, *Mol. Phys.* **2003**, *101*, 2073.
[24] M. Pecul, E. Lamparska, C. Cappelli, L. Frediani, K. Ruud, *J. Phys. Chem. A* **2006**, *110*, 2807.
[25] C. Herrmann, K. Ruud, M. Reiher, *Chem. Phys.* **2008**, *343*, 200.
[26] C. Herrmann, K. Ruud, M. Reiher, *ChemPhysChem* **2006**, *7*, 2189.
[27] P. Bouř, J. Sopková, L. Bednárová, P. Maloň, T. A. Keiderling, *J. Comput. Chem.* **1997**, *18*, 646.
[28] M. Pecul, K. Ruud, *Int. J. Quantum Chem.* **2005**, *104*, 816.
[29] A. J. Thorvaldsen, K. Ruud, *Chirality* **2009**, in press. DOI: 10.1002/chir.20777.
[30] M. Pecul, *Chirality*. in press.
[31] O. Quinet, B. Champagne, *J. Chem. Phys.* **2001**, *115*, 6293.
[32] O. Quinet, V. Liégeois, B. Champagne, *J. Chem. Theory Comput.* **2005**, *1*, 444.
[33] V. Liegeois, K. Ruud, B. Champagne, *J. Chem. Phys.* **2007**, *127*, 204105.
[34] A. J. Thorvaldsen, K. Ruud, K. Kristensen, P. Jørgensen, S. Coriani, *J. Chem. Phys.* **2008**, *129*, 214108.
[35] A. J. Thorvaldsen, K. Ruud, M. Fedorovsky, W. Hug, *Theor. Chim. Acta.* in preparation.
[36] M. Pecul, K. Ruud, Continuum Solvation Models in Chemical Physics, *Continuum Polarized Models*, Wiley-VCH Chichester **2007**.
[37] J. Kapitán, V. Baumruk, V. Kopecký, R. Pohl, P. Bouř, *J. Am. Chem. Soc.* **2006**, *128*, 13451.
[38] L. D. Barron, *Molecular Light Scattering and Optical Activity*, Cambridge University Press: Cambridge, **1982**.
[39] S. Coriani, S. Høst, B. Jansik, L. Thøgersen, J. Olsen, P. Jørgensen, S. Reine, F. Pawlowski, T. Helgaker, P. Sałek, *J. Chem. Phys.* **2007**, *126*, 154108.
[40] E. Cancés, B. Mennucci, J. Tomasi, *J. Chem. Phys.* **1997**, *107*, 3032.
[41] J. Tomasi, M. Persico, *Chem. Rev.* **1994**, *94*, 2027.
[42] J. Tomasi, B. Mennucci, R. Cammi, *Chem. Phys.* **2005**, *105*, 2999.
[43] M. J. Frisch, G. W. Trucks, H. B. Schlegel, G. E. Scuseria, M. A. Robb, J. R. Cheeseman, J. A. Montgomery Jr, T. Vreven, K. N. Kudin, J. C. Burant, J. M. Millam, S. S. Iyengar, J. Tomasi, V. Barone, B. Mennucci, M. Cossi, G. Scalmani, N. Rega, G. A. Petersson, H. Nakatsuji, M. Hada, M. Ehara, K. Toyota, R. Fukuda, J. Hasegawa, M. Ishida, T. Nakajima, Y. Honda, O. Kitao, H. Nakai, M. Klene, X. Li, J. E. Knox, H. P. Hratchian, J. B. Cross, C. Adamo, J. Jaramillo, R. Gomperts, R. E. Stratmann, O. Yazyev, A. J. Austin, R. Cammi, C. Pomelli, J. W. Ochterski, P. Y. Ayala, K. Morokuma, G. A. Voth, P. Salvador, J. J. Dannenberg, V. G. Zakrzewski, S. Dapprich, A. D. Daniels, M. C. Strain, O. Farkas, D. K. Malick, A. D. Rabuck, K. Raghavachari, J. B. Foresman, J. V. Ortiz, Q. Cui, A. G. Baboul, S. Clifford, J. Cioslowski, B. B. Stefanov, G. Liu, A. Liashenko, P. Piskorz, I. Komaromi, R. L. Martin, D. J. Fox, T. Keith, M. A. Al-Laham, C. Y. Peng, A. Nanayakkara, M. Challacombe, P. M. W. Gill, B. Johnson, W. Chen, M. W. Wong, C. Gonzalez, J. A. Pople, *Gaussian 03, Revision A.1*, Gaussian, Inc.: Pittsburgh, PA, **2003**.
[44] S. Miertuš, E. Scrocco, J. Tomasi, *Chem. Phys.* **1981**, *55*, 117.
[45] R. Cammi, J. Tomasi, *J. Comput. Chem.* **1995**, *16*, 1449.
[46] B. Mennucci, E. Cancés, J. Tomasi, *J. Phys. Chem. B* **1997**, *101*, 10506.
[47] Dalton, a molecular electronic structure program, Release 2.0, **2005**, see http://www.kjemi.uio.no/software/dalton/dalton.html.
[48] M. H. Jamróz, Veda 3, Vibrational energy distribution analysis, title, Veda 3. Vibrational Energy Distribution Analysis.
[49] M. Fedorovsky, PyVib2, a program for analyzing vibrational motion and vibrational spectra, **2007**, http://pyvib2.sourceforge.net.
[50] W. Hug, M. Fedorovsky, *Theor. Chim. Acta* **2008**, *119*, 113.
[51] A. Lesarri, E. J. Cocinero, J. C. López, J. L. Alonso, *J. Am. Chem. Soc.* **2004**, *127*, 2572.
[52] M. Pecul, K. Ruud, A. Rizzo, T. Helgaker, *J. Phys. Chem. A* **2004**, *108*, 4269.